JOURNAL OF PHYSICAL ORGANIC CHEMISTRY
J. Phys. Org. Chem. 2001; **14:** 501–512
DOI:10.1002/poc.401

Synthesis of multi-porphyrin arrays and study of their self-assembly behaviour at the air–water interface

Jantien Foekema,[1] Albertus P. H. J. Schenning,[2] Dennis M. Vriezema,[1] Franciscus B. G. Benneker,[1] Kasper Nørgaard,[3] Johannes K. M. Kroon,[4] Thomas Bjørnholm,[3] Martinus C. Feiters,[1] Alan E. Rowan[1]* and Roeland J. M. Nolte[1]

[1]Department of Organic Chemistry, NSR Centre, University of Nijmegen, Toernooiveld 1, 6525 ED Nijmegen, The Netherlands
[2]Department of Chemistry, Eindhoven University of Technology, Den Dolech 2, 5612 AZ Eindhoven, The Netherlands
[3]Centre for Interdisciplinary Studies of Molecular Interactions (CISMI), Chemistry Department–Symbion, University of Copenhagen, Fruebjergvej 3, DK-2100 Copenhagen, Denmark
[4]Department of Organic Chemistry, Wageningen University, Dreijenplein 8, 6703 HB Wageningen, The Netherlands

Received 21 January 2001; Revised 24 April 2001; Accepted 26 April 2001

ABSTRACT: A series of multi-porphyrin arrays were synthesized and the self-assembly behaviour of these compounds at the air–water interface was investigated by the Langmuir–Blodgett technique. It was found that as the overall area of the porphyrin molecules was increased, upon going from a mono- to bis- to a tetra- and then to hexaporphyrin species, the intermolecular stacking between the molecules also increases, resulting in more stable monolayers. In the case of the hexaporphyrin species the intermolecular interactions are so strong that monolayer formation is irreversible. All porphyrin monolayers can be transferred to a glass surface with good transfer ratios, leading to highly ordered porphyrin films in which the chromophores are arranged orthogonal to the glass surface.

KEYWORDS: porphyrins; arrays; self-assembly; air–water interface; monolayers; π–π stacking

INTRODUCTION

The design and construction of self-assembled arrays of chromophoric molecules having well-defined shapes and dimensions is a topic of great current interest, primarily owing to their importance within natural systems, in particular photosynthesis and energy transfer.[1,2] Porphyrins are particularly attractive building blocks for the synthesis of such architectures, since they possess both interesting (photo)catalytic activity and electronic properties.[3,4] As a consequence of these properties, applications can be foreseen in fields such as molecular electronics (molecular-scale wires, switches and photovoltaic devices) and catalysis. Furthermore, these arrays are of great use in the construction of models for the study of the energy- and electron-transfer functions of the natural photosynthetic machinery.[2]

**Correspondence to:* A. E. Rowan, Department of Organic Chemistry, NSR Centre, University of Nijmegen, Toernooiveld 1, 6525 ED Nijmegen, The Netherlands.
E-mail: rowan@sci.kun.nl
Contract/grant sponsor: Dutch Foundation for Chemical Research (CW).
Contract/grant sponsor: Dutch Organization for Scientific Research (NWO).

In earlier work, we described the aggregation behaviour of the Pd-containing porphyrin dimer **5** and the hexaporphyrin species **8** on solid surfaces.[5] Upon evaporation of solutions of these porphyrin-containing molecules on a substrate, ring-shaped assemblies of micrometre size are formed, which can be envisaged as being simple synthetic analogues of the naturally occurring circular photosynthetic antenna complexes LH1 and LH2.[2] These ring structures were studied with several surface scanning techniques such as atomic force microscopy, scanning electron microscopy and near-field scanning optical microscopy, which gave insight into the ordering of the multi-porphyrin molecules within the assemblies.[5] The rings of dimer **5** were found to be constructed from an amorphous conglomerate of smaller nano-sized aggregates whereas the rings formed by hexaporphyrin **8** exhibited a well-defined internal architecture. The increase in structural order found within the rings formed by **8** is partially the result of the large π surface present in the hexaporphyrin species which leads to strong intermolecular π–π interactions between neighbouring porphyrin molecules.

Another approach to organize molecules into ordered arrays is with the help of the Langmuir–Blodgett technique, by which molecules are assembled at an air–water interface.[6] This technique was used in the present study to

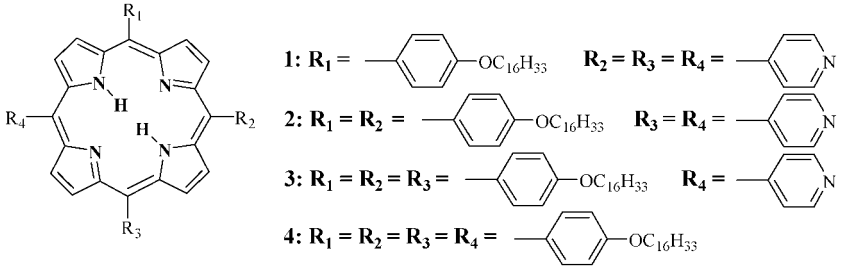

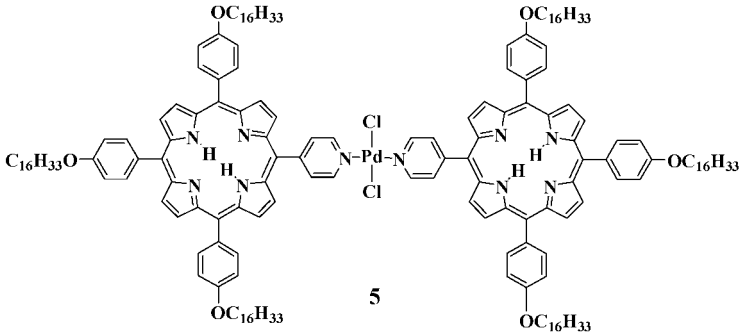

5

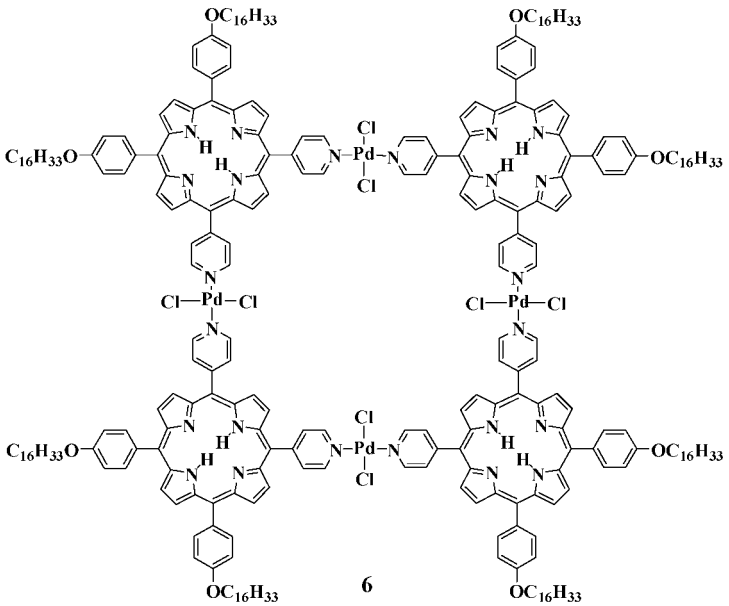

6

investigate the influence of the porphyrin surface area on the self-organizing properties of these molecules. To this end a series of multiporphyrin molecules which possess different porphyrin surface areas were synthesized and studied, i.e. using amphiphilic pyridine porphyrins **1**–**3**,[7] tetrakis(4-hexadecyloxyphenyl)porphyrin **4**,[7] Pd-porphyrin dimer **5**,[7] tetraporphyrins **6** and **7**, which contain Pd and Ru metal centres, respectively, and hexaporphyrins **8**[5] and **9**. Organized mono- and multi-layers of the above-mentioned porphyrins are of potential interest as materials in photoelectric devices and, when derived from chiral porphyrins, as non-linear optical materials.

RESULTS AND DISCUSSION

Synthesis

The amphiphilic porphyrins **1**–**3** were synthesized from 4-(hexadecyloxy)benzaldehyde, 4-pyridinecarboxalde-

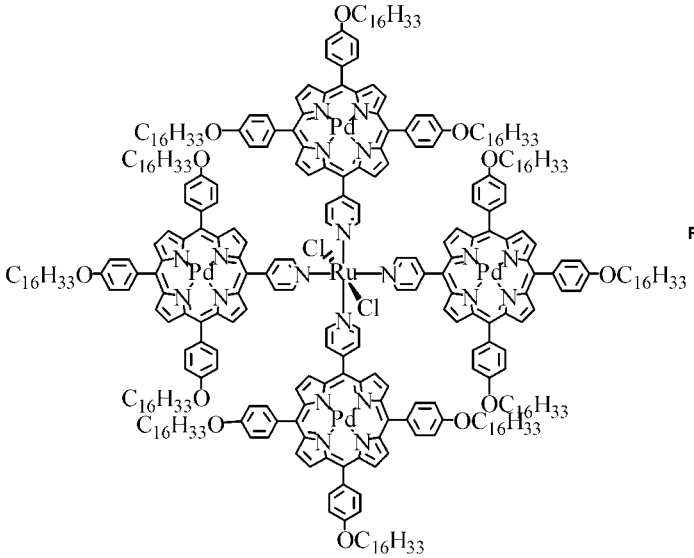

7

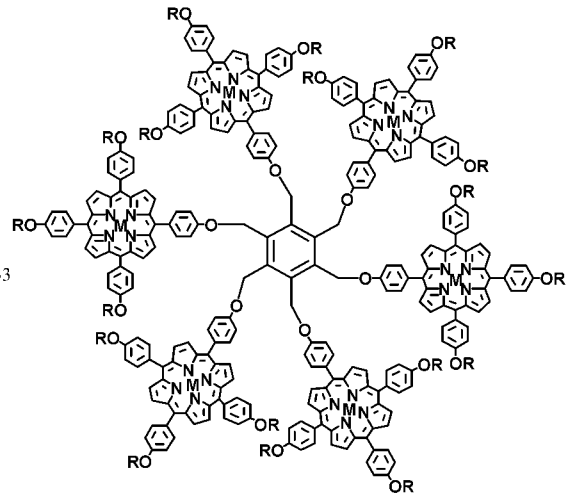

8 : M = 2H
9 : M = Zn(II)

$R = C_{16}H_{33}$

hyde and pyrrole following a method developed in our laboratory.[7,8] Porphyrin **4** was prepared from 4-(hexadecyloxy)benzaldehyde and pyrrole. The multiporphyrin assemblies **5** and **6** were synthesized from *trans*-Pd $Cl_2(NCPh)_2$ and porphyrins **2** and **3**, respectively, following a procedure described by Drain and co-workers.[9] The reactions of these monomeric porphyrins with Pd can be followed by UV–visible spectroscopy. The wavelength maximum of the porphyrin Soret band of **3** was found to shift from 422 to 426 nm upon reaction with the palladium complex and the half-width of this band doubled, in line with the results reported by Drain and co-workers.[9] A titration experiment (Fig. 1) in dichloromethane showed that a well-defined complex with 1:2 Pd to porphyrin stoichiometry was formed.

The titration of *trans*-$PdCl_2(NCPh)_2$ with porphyrin **2** in dichloromethane revealed that a complex with a 1:1 molar ratio was formed (Fig. 2), which is consistent with the expected 4:4 palladium to ligand stoichiometry in complex **6**. In this case the maximum of the Soret band showed a red shift of 8 nm and also a doubling of the half-width of this band was observed. The ability and versatility of this approach to generate well-defined multi-porphyrin arrays has been highlighted by the recent assembly of a nanomeric porphyrin complex.[9]

Porphyrin complexes **5** and **6** could be purified by column chromatography, since they are more apolar than the starting compounds **2** and **3**. Their ^1H NMR spectra showed downfield shifts for the 2′ and 6′ pyridyl protons indicating that the palladium is coordinated to these groups. Both complexes were further characterized by elemental analysis and by mass spectrometry. For porphyrin **6** no mass corresponding to the tetrameric structure was found, probably because the compound is not stable during the mass spectrometric measurement and decomposes. The mass spectra did show, however, the presence of decomposition products, i.e. porphyrin trimers, dimers and monomers. Although, theoretically, larger cyclic arrays would give the same characterization data, due to the geometric constraints imposed by the angle between the pyridines on the porphyrins (90°) and the pyridine–Pd–pyridine angle (180°), no other cyclic structure can be easily formed.

EPR measurements were carried out in order to investigate if there were any electronic interactions between the porphyrin units in molecules of type **5**. For

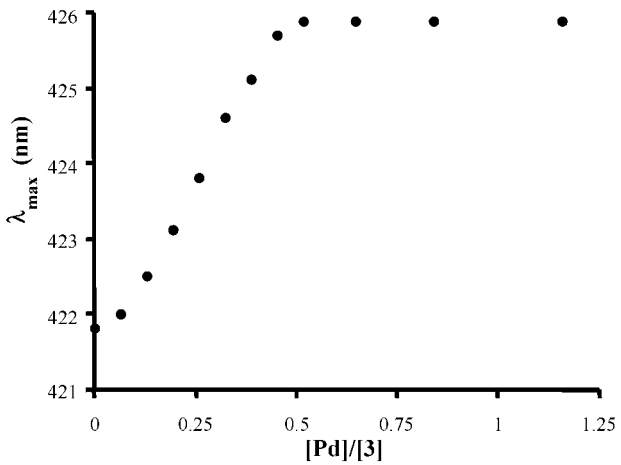

Figure 1. Titration curve describing the complex formation between $PdCl_2(NCPh)_2$ and porphyrin **3** in dichloromethane (for reaction conditions, see Experimental section)

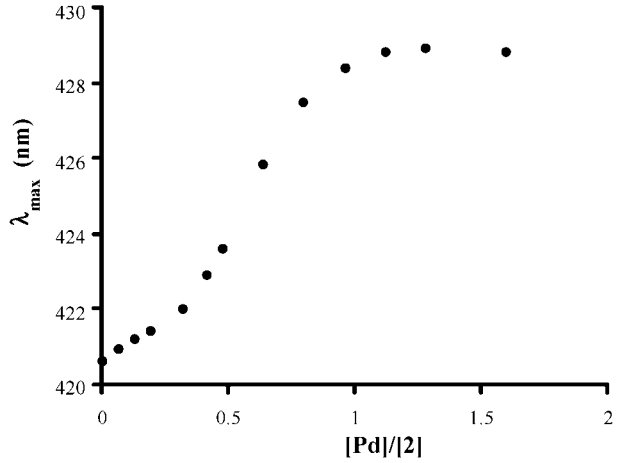

Figure 2. Titration curve describing the complex formation between $PdCl_2(NCPh)_2$ and porphyrin **2** in dichloromethane (for reaction conditions, see Experimental section)

this purpose a copper-containing analogue (**5**·Cu_2) was synthesized by reacting *trans*-$PdCl_2(NCPh)_2$ with Cu-substituted porphyrin **3**. The EPR spectrum of **5**·Cu_2 showed no coupling between the two copper nuclei; only a broadening of the signal relative to the monomer was observed. Based on CPK models, the distance between the copper centres in **5**·Cu_2 was estimated to be approximately 18 Å. This is in line with the observed broadening of the EPR signal, which only occurs when the metal centres are closer than 20 Å.[10,11] Electrochemical studies confirmed that the palladium centres in **5** (and also in **6** without Cu) do not influence each other. A single wave was found in both cases. The reduction potentials of the porphyrins in both complexes were identical [**5**, $E_{1/2} = -1.67$ V; **6**, $E_{1/2} = -1.62$ V (vs Fc/Fc^+)].

Porphyrin **3** was also treated with $RuCl_2(DMSO)_4$ (DMSO = dimethyl sulphoxide),[12] which resulted in another porphyrin tetramer compound **7**. Molecular modelling revealed that steric hindrance between *cis*-porphyrins in **3** leads to a non-planar arrangement of the chromophores, unlike in **5** and **6** (see Fig. 3). The chloride ligands in **7** are orthogonal to the plane of the molecule (also unlike in **5** and **6**). The maximum of the Soret band of **7** was found to be red shifted and the width at half-height of this band was found to be increased when compared with **3**. The ^1H NMR spectra of **7** revealed downfield shifts for the 2′ and 6′ protons of the pyridyl groups indicating that the ruthenium(II) centre is coordinated to these groups. The complex was further characterized by elemental analysis.

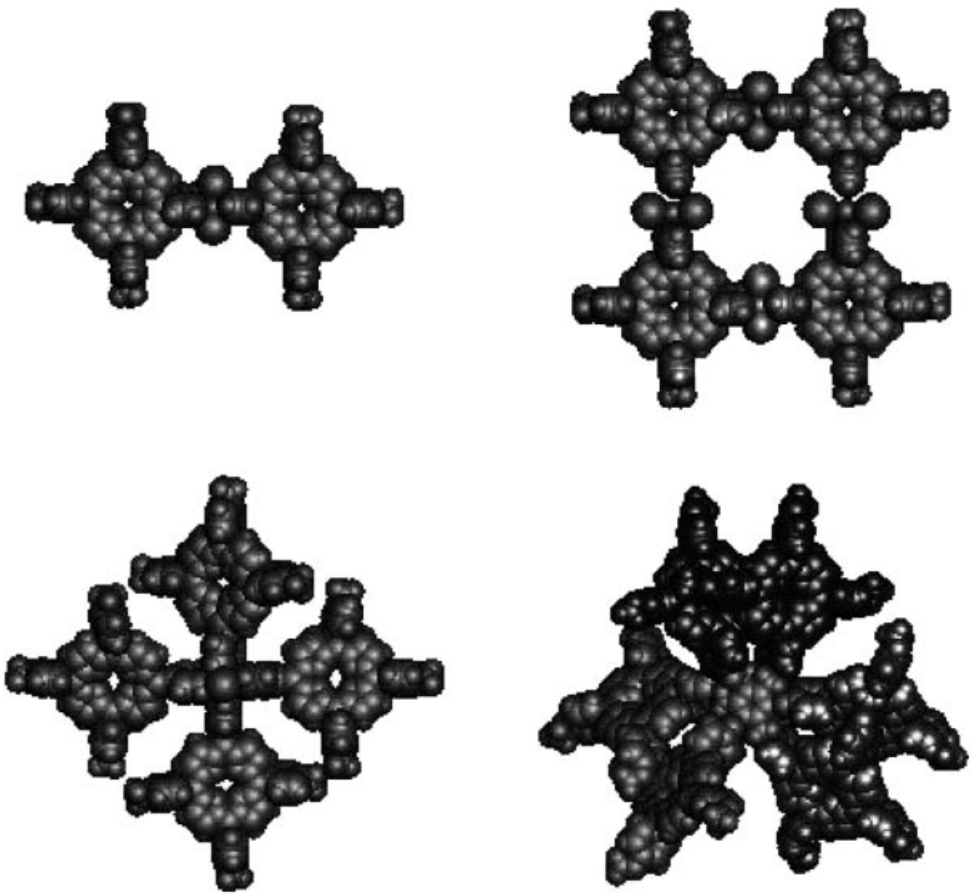

Figure 3. Space-filling representations of the multi-porphyrin molecules; bisporphyrin **5** (top left), tetraporphyrin **6** (top right), ruthenium tetraporphyrin **7** (bottom left) and hexaporphyrin **8** (bottom right)

It is known that tetrakis(pyridinium)ruthenium(II) dichloride can be reversibly oxidized in acetonitrile at a potential of 0.26 V vs SCE.[12] For **7**, however, no oxidation wave for the oxidation of ruthenium(II) to ruthenium(III) was observed around this potential. This puzzling result is attributed to the 12 long aliphatic chains present in this molecule. Molecular modelling studies suggested that the ruthenium metal in **7** could be completely shielded by the tails of the amphiphilic porphyrin units, which may cause an inhibition of the electron transfer process at the electrode. Furthermore, it was found that the reduction of the porphyrin units was irreversible which also may be the result of the shielding effect of the hydrocarbon chains. Encapsulated porphyrins[13] and dendrimeric porphyrins[14] have been reported previously to display a similar irreversible electrochemical response.

Hexaporphyrin **8** was synthesized by a base-catalysed coupling reaction of 5-(4-hydroxyphenyl)-10,15,20-(4-hexadecyloxyphenyl)porphyrin to hexakis(bromomethyl)benzene. The compound was fully characterized by elemental analysis and NMR and mass spectrometry. NMR measurements and molecular modelling studies were performed to obtain information about the overall structure of **8** and the geometric arrangement of the porphyrins in this molecule.[5] These studies revealed that the porphyrins are arranged in dimeric pairs around the central benzene ring with an average centre-to-centre distance of 9 Å, giving the molecule a propeller-like shape. As in the case of **5**, EPR experiments were carried out on the Cu derivative of **8**. No coupling between the metal centres was observed, indicating that the copper–copper distance must be larger than 6 Å. The EPR signals were broadened, however, which suggests that the two metal centres are less than 20 Å apart. On going from 5-(4-hydroxyphenyl)-10,15,20-(4-hexadecyloxyphenyl)porphyrin to hexamer **8** no shifts in wavelength in the UV–visible spectra were observed. Only a slight broadening of the Soret band at $\lambda_{max} = 423$ nm of **8** was visible, implying that no significant electronic interactions are present between adjacent porphyrins in this molecule. This is in line with the calculated centre-to-centre distance of 9 Å, which is too large for excitonic coupling to occur.

Reaction of **8** with $Zn(OAc)_2$ yielded the hexazinc(II) porphyrin **9** in almost quantitative yields. NMR spectrometry for this compound revealed similar chemical shifts as found for **8**,[5] indicating that **8** and **9** possess a similar non-planar, propeller-like geometry (Fig. 3). UV–visible studies, however, revealed a small (3 nm) blue shift of the zinc(II) porphyrins in **9**, compared with the monomeric zinc(II) derivative of 5-(4-hydroxyphenyl)-10,15,20-(4-hexadecyloxyphenyl)porphyrin. According to the exciton model developed by Kasha and co-workers,[15] a blue shift points to a face-to-face stacking of porphyrins. Apparently, the pairs of zinc(II)porphyrins in **9** are more overlapping (on top of each other) than the pairs of free base porphyrins in **8**, resulting in a smaller overall porphyrin surface area for the former molecule.[16]

Langmuir monolayers and Langmuir–Blodgett multilayers

In a previous paper, we reported on the physical properties of monolayers formed by **1–4**.[8] In the following monolayer studies on porphyrins **5–9** using the Langmuir–Blodgett (film balance) technique are described

The characteristic features of the Langmuir monolayers of compounds **5–9** and for comparison also from compounds **1–4** are listed in Table 1. The organization and orientation of the porphyrins in the monolayers is determined by the balance between the intermolecular π–π interactions, the interaction of the hydrophilic (pyridine) groups with the aqueous phase and the steric repulsion between the hydrocarbon chains. As we

Table 1. Molecular area, compressibility (α), transfer properties and UV–visible data for monolayers of amphiphilic porphyrins **1–9**

Compound	Molecular area[a]	α (mN m^{-1})$^{-1}$	Type of transfer	Transfer ratio		Soret-band (nm)[b]		
				Downstroke	Upstroke	$CHCl_3$	Air–water	Glass
1[c]	60	0.004	Z	<0.2	>0.6	426	445	—
2[c]	88	0.008	Y	0.7–0.9	1.0	420	432	—
3[c]	115	0.017	Y	>0.8	1.0	420	398/440	—
4	50	0.015	—	—	—	420	398/440	—
5	360	—	—	—	—	426	—	—
6	360	0.008	Z	0.1	0.6	426	430[d]	—
7	800	0.05	—	—		422	—	—
8	200	—	—			423	436	436
9	200	—	—	0.69		423	436	436

[a] The mean molecular areas (Å^2 per molecule) were determined by taking the tangent of the isotherms at the pressure of the monolayer transfer (10 mN m^{-1}) and extrapolating to zero pressure.
[b] The UV–visible spectra were recorded after equilibration of the monolayer.
[c] Taken from Ref. 6.
[d] Asymmetric band with a shoulder at 416 nm.

reported previously, the take-off area of compounds **1**–**4** gradually increases upon increasing number of alkyl chains from one (**1**) to three (**3**) hydrocarbon tails (Table 1).[7] The molecular areas as predicted from CPK models (CPK models, Harvard Apparatus; all computational calculations were carried out using the CHARMM 3.31 force field within the QUANTA package) are significantly larger than the measured areas derived from the isotherms, which indicates that the planes of porphyrins **1**–**4** are tilted (even orthogonal for molecule **4**) with respect to the water surface. We propose that the polar pyridine groups point to the aqueous interface and determine the orientation of the porphyrins at this interface. The number of hydrocarbon chains subsequently determines the distance between the porphyrins within the monolayer, which results in an increase in the mean molecular area from 60 to 115 $Å^2$ per molecule on going from **1** to **3**. With a very small measured molecular area of 50 $Å^2$ per molecule, which points to an almost perpendicular orientation on the water surface, porphyrin **4** does not follow this trend. This can be understood, since **4** possesses no polar pyridyl groups to interact with the water surface, and hence the organization of the molecules in the monolayer is determined solely by intermolecular forces.

Dimer **5** showed a rise of the surface pressure at an area of 360 $Å^2$ per molecule (Table 1). Already above 6 mN m^{-1} the monolayers collapsed, indicating that they are not stable (isotherm not shown). For tetramer **6** an identical take-off area of 360 $Å^2$ per molecule was measured (Fig. 4), suggesting that its molecules are aligned at the air–water interface in a similar way to those of compound **5**. In contrast to **5**, however, the monolayers assembled from **6** were far more stable. The molecular areas measured for **5** and **6** indicate that the planes of the molecules are also tilted with respect to the interface with two porphyrin units pointing to the water surface. The difference in stability of the monolayers of tetraporphyrin **6** compared with those of diporphyrin **5** can be attributed to the two extra porphyrin units present in the former compound. The larger π surface is thought to give an extra stabilizing interaction between neighbouring molecules of **6**, which prevents the porphyrin monolayers from collapsing.

For tetraporphyrin **7** a completely different surface pressure isotherm was recorded. A rise of surface pressure was already observed at 800 $Å^2$ per molecule, indicating that the molecules are initially lying flat on the air–water interface. The lipophilic hydrocarbon chains presumably adopt an orientation perpendicular to this interface. During further compression the porphyrin units were lifted from the water surface and at an area of 100 $Å^2$ per molecule a second steep increase of the surface pressure was observed. This second rise of surface pressure corresponds to twice the molecular area measured for porphyrin **4**. This may indicate that **7** is also oriented perpendicular to the air–water interface with one or possibly two porphyrin units making contact with the water surface in a similar orientation as seen for the molecules in the monolayers of **2**–**4** (Fig. 5). The fact that the porphyrin **7** initially lies flat on the water surface might be attributed to the interaction of the ruthenium(II) centre with the water sub-phase.

To study the organization of the propeller shaped hexaporphyrins **8** and **9**[5] on the water subphase, solutions of these compounds in chloroform (10^{-4}–10^{-3} M) were spread on water, and after evaporation of the solvents the isotherms were measured. Compounds **8** and **9** showed a rise in surface pressure at 200 and 250 $Å^2$ per molecule, respectively (Fig. 4). With the diameter of the molecules

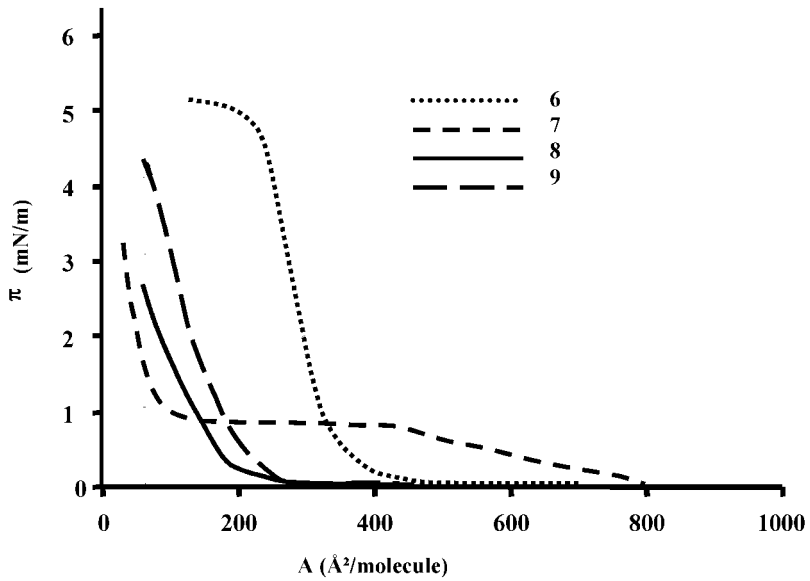

Figure 4. Surface pressure isotherms of the amphiphilic porphyrin multimers **6**, **7**, **8** and **9** on pure water at room temperature

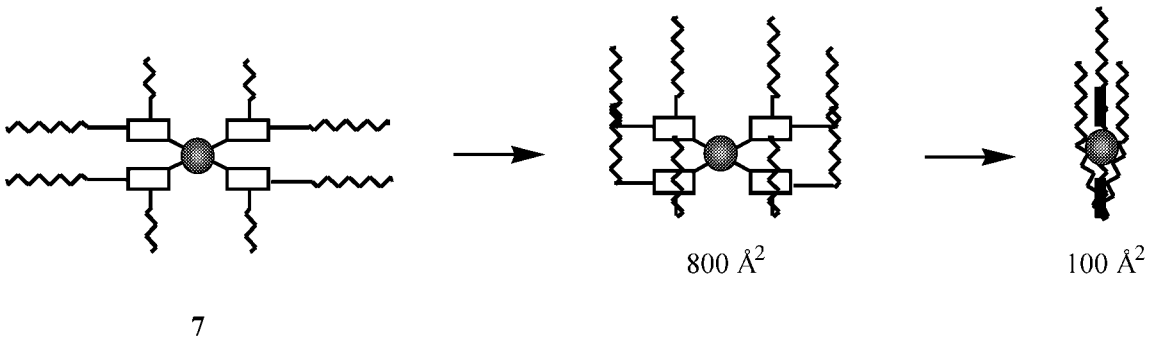

Figure 5. Schematic representations of the proposed conformations of **7** in a monolayer at the air–water interface at different surface pressures

being 50 Å (predicted from CPK models) and hence the calculated area being 2500 $Å^2$, the measured take-off areas point in both cases to a perpendicular orientation of the disc-shaped molecules with respect to the water subphase. Furthermore, these areas indicate that the distances between the molecules of **8** and **9** amount to 4 and 5 Å, respectively. These distances are small enough for inter-excitonic coupling to occur.

UV–visible spectroscopy on the monolayer at the air–water interface revealed before compression a 16 nm red-shifted Soret band for both hexamers **8** and **9** with respect to their solution spectra, which is indicative of an off-set, edge-to-tail arrangement of the porphyrins. This shift implies that the hexaporphyrin molecules self-assemble immediately upon spreading on the surface prior to compression, forming small domains on the water surface. Compression merely results in an increase in the observed absorption due to an increase in the local concentration of the chromophores, which is a result of the small domains being pushed together. The red shift of the Soret band was unaltered upon further compression and hence the arrangement of hexaporphyrins within the small preformed domains remained intact (Fig. 6). This observation is not uncommon for monolayers of porphyrins, especially when they are as hydrophobic as **8**.[5] There is a very little favourable interaction between the hydrophobic hexaporphyrins and the water subphase, which induces the molecules to aggregate immediately after deposition. The organization and orientation of the molecules in the aggregates are determined by intermolecular forces (mainly π–π interactions and the interactions of the alkyl tails). It should be noted that a large

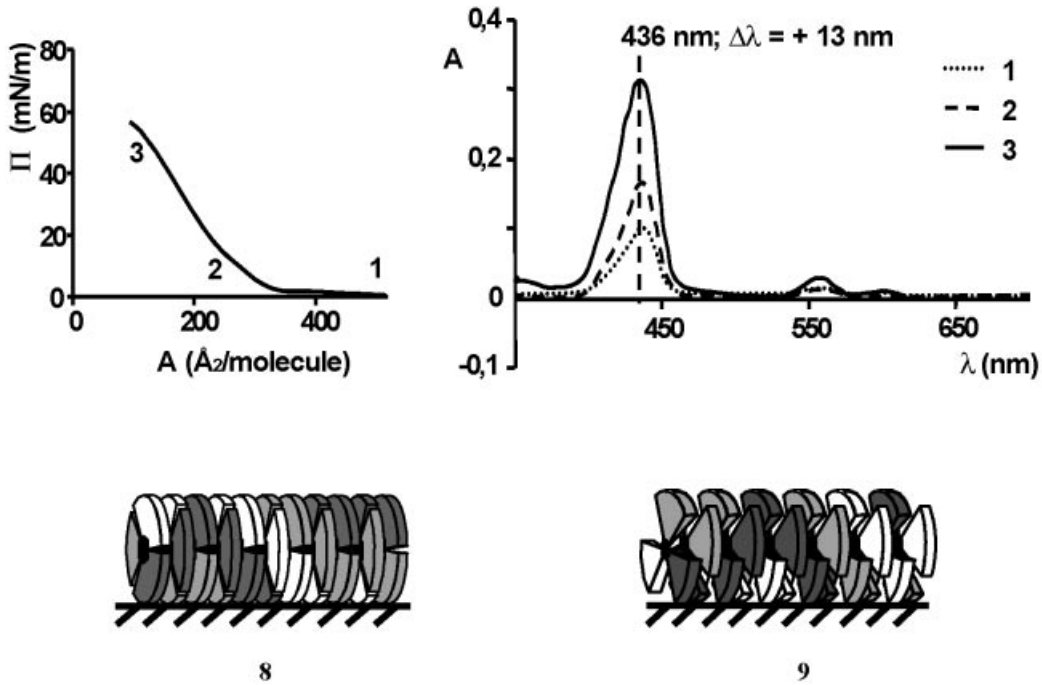

Figure 6. Top left: isotherm recorded for **9** and the corresponding UV–visible spectra (top right) at different stages during compression. Bottom: proposed stacked orientation of **8** (left) and **9** (right) within the monolayer

volume fraction is due to the alkyl tails. In the case of the tetramers **6** and **7** they possess 12 tails whereas **8** and **9** possess 18 alkyl tails. These alkyl tails also play a significant role in the monolayer stability.

The observed red shift in the case of **8** and **9** can either arise from intermolecular stacking or be the consequence of intramolecular stacking within one hexaporphyrin. Zinc(II) derivative **9** displayed a shifted Soret band in solution, which was blue shifted compared with that of a control monomeric porphyrin, which indicates intramolecular stacking of the porphyrins in a face-to-face arrangement. When the porphyrins within one hexamer are pushed together, the blue shift can be expected to become more pronounced. As shown in Fig. 6, for **9** this is not the case. Instead, a redshift is observed, indicative of an edge-to-tail orientation of the porphyrins. This red shift must be the result of intermolecular exciton coupling, not intramolecular interactions. These observations lead to the idea that the neighbouring hexaporphyrins are arranged in columns. Within the columns the molecules are slightly rotated with respect to each other in order to accomplish an edge-to-tail ordering of the porphyrins within one 'hexamer' with the porphyrins of a neighbouring 'hexamer' (Fig. 6, bottom).

Hysteresis experiments were performed in order to obtain information about the reversibility of monolayer formation. These experiments showed that monolayers of **8** were irreversibly formed, in contrast to those of **9**, which were reversibly formed (Fig. 7). This difference may be attributed to the difference in stacking forces between the hexaporphyrins. As was deduced from the UV–visible experiments described above, the free base porphyrins in **8** span a larger area within the molecule, providing more stacking possibilities with neighbouring molecules, than is possible for the zinc(II) porphyrins in **9**. The latter are face-to-face ordered within one molecule of **9**, resulting in a smaller porphyrin surface area and hence less π–π stacking interaction with other hexaporphyrins, resulting in reversible monolayer formation. In addition, the zinc centre in **9** is able to complex weakly an axial ligand forming a five-coordinate zinc species. Upon deposition on a water interface the zinc could readily complex a water molecule which would interfere with optimal π–π stacking. Contradictory to this argument, however, are the identical red shifts observed for both **8** and **9** upon aggregation, which indicate a similar intermolecular stacking geometry. Probably both the more compact molecular geometry of **9** when compared with **8** and the possibility of coordinating a water molecule are responsible for the larger molecular area found for the former compound and the reversible formation of its monolayer.

The values of the compressibility parameter, α, for some of the porphyrin multimers are included in Table 1.[18] As can be seen, the monolayer of tetraporphyrin **7** has a more fluid character than the monolayer of tetraporphyrin **6**. Transfer of the monolayers of compound **6** to hydrophilic glass substrates was studied at a surface pressure of 20 mN m^{-1}. At higher pressures collapse of the layers occurred. The transfer properties of this porphyrin are also compiled in Table 1. Low downstroke and upstroke transfer ratios are observed which are most likely due to the weak interaction of the apolar porphyrin **6** with the hydrophilic glass. The UV–visible absorption spectrum of transferred **6** showed an asymmetric Soret band, which indicates some splitting of this band and presumably the formation of edge-to-edge type of aggregates.[15] Brewster angle microscopy experiments on the monolayers of **6** revealed that after spreading the porphyrin molecules formed domains and after compression a homogeneous film.[7] By applying an equilibration period of 15 min at a surface pressure of 0 mN m^{-1} a homogeneous film was obtained. UV–visible spectroscopy indicated that **6**, just like **8** and **9**, formed aggregates immediately after spreading.

Transfer of the monolayers on to a substrate was also investigated using hexaporphyrin **8**. Both hydrophilic and hydrophobic quartz substrates were used in order to

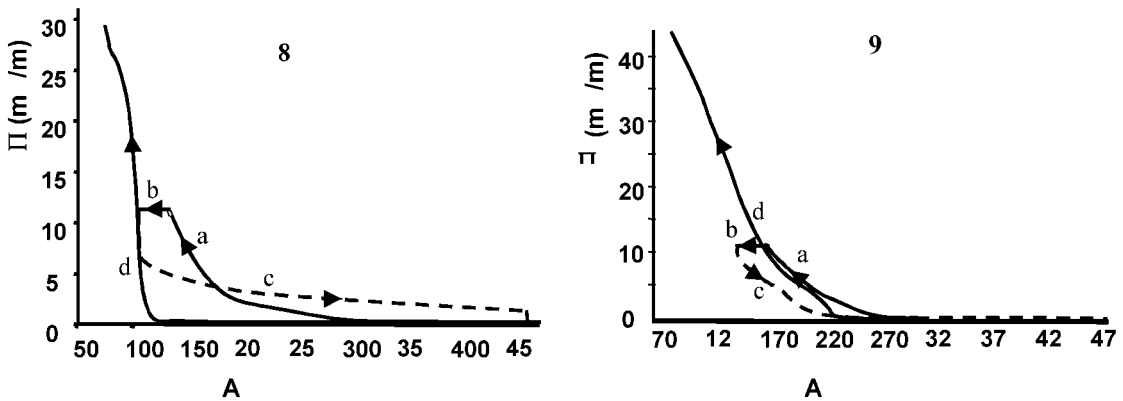

Figure 7. Hysterisis experiments on Langmuir–Blodgett monolayers containing free base hexaporphyrin **8** (left) and Zn hexaporphyrin **9** (right). Initial compression (a), stabilization (b), removal of pressure (c) and recompression (d)

investigate the influence of the nature of the surface on the transfer. The dipped substrates were further studied using UV–visible spectroscopy.

In contrast to what was expected, because **8** is highly hydrophobic, transfer of this compound on to the hydrophobic quartz slides was very poor. Vertical dipping had to be repeated 10 times in order to obtain sufficient transfer of material and the prepared film was very irregular. Transfer of the monolayer by vertical dipping on to hydrophilic quartz substrates was also poor. The specific character of the monolayer with very strong π–π interactions between molecules is thought to hinder transfer. Probably upon lowering the quartz substrate into the monolayer a hole is created, which is not refilled with new hexamer material. Horizontal dipping using a hydrophilic quartz substrate proved to be the most successful procedure, as was concluded from the observed selectively high UV–visible absorption intensity.

All the dipped substrates containing a film of **8** displayed a red shift of the Soret band, indicative of edge-to-tail stacking of the porphyrins (Fig. 8), similar to the red shift observed for the monolayers on a water subphase. Apparently, the orientation of the hexaporphyrin molecules with respect to each other is preserved upon transfer, although the ordering decreases, as is evidenced by the significant broadening of the Soret band. This decrease in ordering can be attributed in part to the poor transfer ratio. In spite of this poor transfer ratio by studying the substrates under different angles with respect to the light source of the UV–visible apparatus, it was concluded that the plane of the porphyrins in the hexaporphyrin molecules is perpendicular to the quartz substrate, just as it is on the water surface itself with the hexaporphyrins arranged in small domains (see Fig. 8, bottom).

CONCLUSIONS

We have shown that it is possible to assemble multi-porphyrin compounds in monolayers on a water surface. These monolayers can endure surface pressures from 50 to 60 mN m^{-1} before collapse occurs. The porphyrin

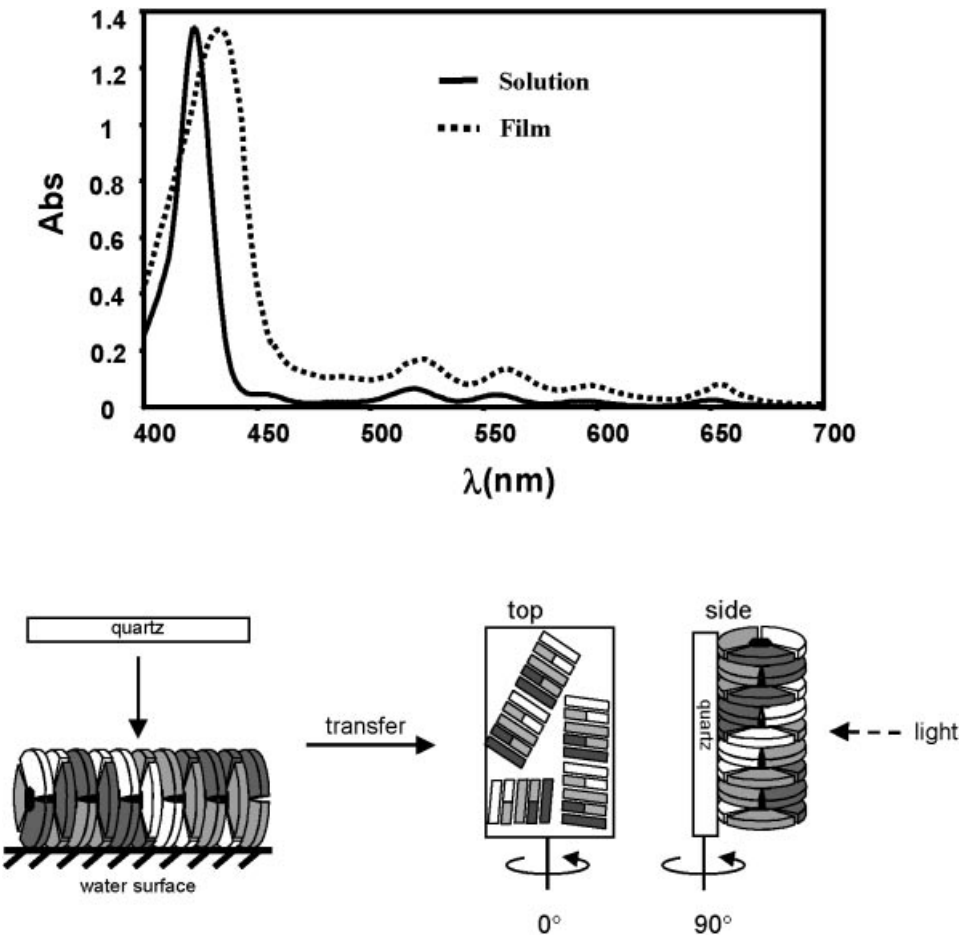

Figure 8. (Top) UV–visible spectra of hexaporphyrin **8** in chloroform solution and in a monolayer deposited on a hydrophilic glass slide (3× vertical dipping). (Bottom) schematic representation of the horizontal transfer of a monolayer of **8** from the water surface on to a hydrophilic quartz slide

molecules described adopt a perpendicular orientation with respect to the water surface. Compounds **5** and **6** are tilted and **7** is initially lying flat on this surface, but is lifted upon further compression. Except for **5**, the monolayers are fairly stable and can be transferred on to hydrophilic glass substrates, as was demonstrated with compounds **6**, **8** and **9**. The size of the porphyrin surface has an influence on the stability of the monolayer. This is evident when bisporphyrin **5** is compared with the tetraporphyrin **6**. The two extra porphyrin moieties in the latter compound lead to a more stable monolayer. Tetraporphyrin **7** displays a deviating behaviour and cannot be fitted in these comparisons. Hexaporphyrins **8** and **9**, which possess the largest surface area, form the most tightly aggregated monolayers, in spite of being non-planar. The intermolecular π–π stacking and the interactions of the alkyl tails for compound **8** results in such a strong intermolecular interaction that its monolayers are irreversibly formed.

EXPERIMENTAL

Unless indicated otherwise, commercial materials were used as received. $CHCl_3$ was distilled from calcium hydride. Melting-points were measured with a Jeneval polarising microscope connected to Linkam THNS 600 hot-stage. Fast atom bombardment (FAB) mass spectra were recorded with a double focusing VG 7070E spectrometer. As a matrix nitrobenzyl alcohol was used. EPR spectra were recorded on a Bruker ESP 300 spectrometer, equipped with an Oxford flow cryostat. Elemental analyses were performed with a Carlo Erba Ea 1108 instrument. ^{1}H NMR spectra were recorded on Bruker WH-90, WM-200 and AM-400 instruments. Chemical shifts (δ) are reported in ppm downfield from the internal standard tetramethylsilane. Abbreviations used are s = singlet, d = doublet, t = triplet, m = multiplet and br = broad. Thin-layer chromatography (TLC) was performed using precoated F-254 plates and column chromatography using basic alumina and silica 60H (Merck). *trans*-Bis(benzonitrile)palladium(II) dichloride was purchased form Acros Chimica. Tetrakis(dimethylsulphoxide)ruthenium(II) dichloride 21,23-2*H*-5-(4-pyridyl)-10,15,20-tri(4-hexadecyloxyphenyl)porphyrin (**1**), 21,23-2*H*-5,10-di(4-pyridyl)-15,20-di(4-hexadecyloxyphenyl)porphyrin (**2**) and hexakisporhyrinatobenzene (**8**) were synthesized according to literature procedures.[5,17]

*Bis[21,23-2H-5-(4-pyridyl)-10,15,20-tri(4-hexadecyloxyphenyl)porphyrin]palladium dichloride (**5**).* *trans*-Bis(benzonitrile)palladium(II) dichloride (7.2 mg, 0.018 mmol) was added with stirring to a solution of **3** (50 mg, 0.037 mmol) in 50 ml of dichloromethane. After 2 h the solvent was evaporated and the resulting solid was adsorbed on silica. Compound **5** was subsequently purified isolated by elution with $CHCl_3$–MeOH (95:5, v/v). Yield: 34 mg (64%). TLC [silica, MeOH–$CHCl_3$ (5:95, v/v)], $R_f = 0.95$. m.p.: 225 °C (decomposition to starting materials). IR (KBr, cm^{-1}): 3433, 2923, 2852. ^{1}H NMR (200 MHz, $CDCl_3$), δ: 9.58 (d, 4H, pyridyl, $J = 6.6$ Hz), 8.99 (s, 4H, β-pyrrole, $J = 4.9$ Hz), 8.89 (s, 8H, β-pyrrole), 8.82 (d, 4H, β-pyrrole, $J = 4.9$ Hz), 8.37 (d, 8H, pyridyl, $J = 6.6$ Hz), 8.18 (d, 12H, phenyl, $J = 8.4$ Hz), 7.45 (d, 12H, phenyl, $J = 8.4$ Hz), 4.40 (t, 12H, OCH_2, $J = 2.6$ Hz), 2.0–1.3 (b, 168H, CH_2), 1.00 (t, 18H, CH_3), −2.75 (b, 4H, NH). FD MS: found for $C_{182}H_{250}N_{10}O_6Pd$ *m/z* 2776.86576; calc. 2776.86156. UV–vis ($CHCl_3$), λ/nm log(ε/l mol^{-1} cm^{-1})): 426(5.9), 521(4.6), 558(4.5), 592(4.2), 651(4.2). Anal. Calc. for $C_{182}H_{248}N_{10}O_6PdCl_2$, C 76.72, H 8.77, N 4.92; found, C 76.59, H 8.96, N 4.85%. CV: $E_{1/2} = -1.67$ V (vs Fc/Fc$^+$), $\Delta E_p = 69$ mV, $E_{1/2} = -1.98$ V, $i_b/i_f = 1$.

Copper(II) 5-(4-pyridyl)-10,15,20-tri(4-hexadecyloxyphenyl)porphyrin. This compound was synthesized according to a literature procedure.[5] Yield: 95%. UV–vis ($CHCl_3$), λ/nm (log(ε/l mol^{-1} cm^{-1})): 418(5.5), 540(4.2). FAB-MS: *m/z* = 1398 (M).

Bis[copper(II) 5-(4-pyridyl)-10,15,20-tri(4-hexadecyloxyphenyl)porphyrin]palladium(II) chloride. This compound was synthesized in the same way as described for compound **5**. Yield: 53%. UV–Vis ($CHCl_3$), λ/nm (log(ε/l mol^{-1} cm^{-1})): 422(5.7), 540(4.6). Anal. Calc. for $C_{182}H_{246}N_{10}O_6Cu_2PdCl_2 \cdot H_2O$, C 73.05, H 8.35, N 4.68; found, C 72.71, H 8.31, N 4.73%.

*Tetra(21,23-2H-5,10-di(4-pyridyl)-15,20-di(4-hexadecyloxyphenyl)porphyrin tetra(palladium dichloride) (**6**).* *trans*-Bis(benzonitrile)palladium(II) dichloride (19 mg, 0.048 mmol) was added with stirring to a solution of **2** (55 mg, 0.049 mmol) in 50 ml of dichloromethane. After 2 h the solvent was evaporated and the resulting solid was adsorbed on silica. Compound **6** was isolated by column chromatography [eluent $CHCl_3$–MeOH (95:5, v/v)]. Yield: 29 mg (47%). TLC [silica, MeOH–$CHCl_3$ (5:95, v/v)], $R_f = 1$. M.p. >400 °C. IR (KBr, cm^{-1}): 3433, 2923, 2852. ^{1}H NMR (200 MHz, $CDCl_3$), δ: 9.50 (d, 16H, pyridyl, $J = 6.2$ Hz), 8.9 (m, 24H, β-pyrrole), 8.34 (d, 16H, pyridyl, $J = 6.2$ Hz), 8.15 (d, 16H, phenyl, $J = 8.26$ Hz), 7.35 (d, 16H, phenyl, $J = 8.57$ Hz), 4.3 (t, 16H, OCH_2), 2.0–1.3 (b, 224H, CH_2), 0.9 (t, 24H, CH_3), −2.8 (b, 8H, NH). FD MS: found for dimer $C_{148}H_{184}N_{12}O_4Pd_2Cl_2$, *m/z* = 2473.20421; calc. 2473.20850. UV–Vis ($CHCl_3$), λ/nm (log(ε/l mol^{-1} cm^{-1})): 429(6.0), 520(4.7), 556(4.5), 592(4.3), 648(4.0). Anal. calc. for $C_{296}H_{368}N_{24}O_8Pd_4Cl_8$, C 69.72, H 7.27, N 6.59; found, C 69.66, H 8.22, N 6.42%. IR (KBr, cm^{-1}): 3433, 2923, 2852. CV: $E_{1/2} = -1.62$ V (vs Fc/Fc$^+$), $\Delta E_p = 82$ mV, $i_b/i_f = 1$.

Palladium(II) 5-(4-pyridyl)-10,15,20-tri(4-hexadecyloxyphenyl)porphyrin. This compound was synthesized

according to a literature procedure.[17] Yield: 90%. ^{1}H NMR (200 MHz, $CDCl_3$), δ: 9.00 (d, 2H, pyridyl, $J = 5.8$ Hz), 8.88 (d, 2H, β-pyrrole, $J = 5.0$ Hz), 8.86 (s, 4H, β-pyrrole), 8.72 (d, 2H, β-pyrrole, $J = 5.0$ Hz), 8.12 (d, 2H, pyridyl, $J = 5.9$ Hz), 8.05 (d, 6H, phenyl, $J = 8.3$ Hz), 7.25 (d, 6H, phenyl, $J = 8.4$ Hz), 4.20 (t, 6H, OCH_2), 2.10 (m, 6H, OCH_2CH_2), 1.6–1.2 (m, 78H, CH_2) 0.90 (t, 9H, CH_3). UV–Vis ($CHCl_3$), λ/nm ($\log(\varepsilon/l\ mol^{-1}\ cm^{-1})$): 419(5.1), 524(4.0). FAB MS: $m/z = 1441$ (M + 1).

*Tetrakis[palladium(II) 5-(4-pyridyl)-10,15,20-tri(4-hexadecyloxyphenyl)porphyrin]ruthenium(II) dichloride (**7**).* Palladium(II) 5-(4-pyridyl)-10,15,20-tri(4-hexadecyloxyphenyl)porphyrin (20 mg, 14 mmol) and $RuCl_2(DMSO)_4$ (1.7 mg) were reacted in the melt ($T = 90$ °C) for 30 min. Purification was achieved by column chromatography (eluent CH_2Cl_2). Yield: 8.5 mg (45%). M.p. = 97 °C (decomposition to starting materials). ^{1}H NMR (200 MHz, $CDCl_3$), δ: 9.75 (d, 8H, pyridyl, $J = 6.1$ Hz), 9.01 (d, 8H, β-pyrrole, $J = 4.9$ Hz), 8.86 (d, 8H, β-pyrrole), 8.81 (s, 16H, β-pyrrole), 8.35 (d, 8H, pyridyl, $J = 6.5$), 8.10 (d, 8H, phenyl, $J = 8.6$ Hz), 8.00 (d, 16H, phenyl, $J = 8.5$ Hz), 7.26 (d, 8H, phenyl, $J = 8.5$ Hz), 7.08 (d, 16H, phenyl, $J = 8.6$ Hz), 4.24 (t, 8H, OCH_2, $J = 5.9$ Hz), 4.01 (t, 16H, OCH_2, $J = 6,2$ Hz), 2.00–1.30 (b, 336H, CH_2), 0.88 (t, 36H, CH_3, $J = 6.9$ Hz). UV–Vis ($CHCl_3$), λ/nm ($\log(\varepsilon/l\ mol^{-1}\ cm^{-1})$): 422(6.1), 527(4.9), 556(4.51). Anal. calc. for $C_{364}H_{492}N_{20}O_{12}Pd_4RuCl_4$, C 72.57, H 8.37, N 4.66; found, C 72.76, H 8.25, N 4.67%.

*Hexakis[zinc(II) porphyrinatobenzene] (**9**).* A solution of hexaporphyrin **8** (14.4 mg, 1.75 μmol) and $Zn(OAc)_2 \cdot 2H_2O$ (25 mg, 0.11 mmol) in 25 ml of $CHCl_3$–CH_3OH (2:1) was refluxed for 2 h. After evaporation the product was purified by column chromatography (eluent $CHCl_3$). Yield: 13.9 mg (92%). M.p. = 185 °C. ^{1}H NMR (300 MHz, $CDCl_3$), δ: 8.96 (d, 12H, β-pyrrole, $J = 4.7$ Hz), 8.94 (d, 12H, β-pyrrole), 8.65 (d, 12H, β-pyrrole, $J = 4.6$ Hz), 8.44 (d, 12H, phenyl, $J = 7.8$ Hz), 8.18 (d, 12H, phenyl, $J = 8.1$ Hz), 8.02 (d, 12H, β-pyrrole, $J = 4.3$ Hz), 7.79 (d, 12H, phenyl, $J = 8.5$ Hz), 7.30 (d, 12H, phenyl, $J = 7.5$ Hz), 6.86 (d, 24H, phenyl, $J = 7.7$ Hz), 6.25 (s, 12H, benzyl), 5.81 (d, 24H, phenyl, $J = 8.0$ Hz), 4.28 (br, 12H, OCH_2), 3.01 (br, 24H, OCH_2), 2.0–1.1 (br, 504H, CH_2), 0.86 (br, 54H, CH_3). MALDI-TOF-MS: $m/z = 8665$ [$M^+ + Na$]. Anal. calc. for $C_{564}H_{750}N_{24}O_{24}Zn_6$, C 78.38, H 8.75, N 3.89; found, C 79.29, H 8.12, N 3.61%.

Field desorption mass spectrometry. This technique was applied for measuring the masses of compounds **5, 6** and **7** because FAB-MS only showed decomposition products. Field desorption (FD) mass spectrometry was carried out using a JEOL JMS SX/SX102A four-sector mass spectrometer, coupled to a JEOL MS-MP7000 data system; 10 μm tungsten wire FD emitters containing carbon microneedles with a average length of 30 μm were used. The samples were dissolved in methanol–water and then loaded on to the emitters with the dipping technique. An emitter current of 0–15 mA was used to desorb the samples. The ion source temperature was generally 90 °C.

UV–visible titration experiments. A stock solution of porphyrin in dichloromethane was prepared (concentration 1.3×10^{-6} M). Exactly 2 ml of this solution were transferred to a quartz cuvette (pathlength 1.000 cm) in a thermostated compartment of a Perkin-Elmer λ-5 UV–visible spectrophotometer. Subsequently, 25 μl aliquots of a *trans*-bis(benzonitrile)palladium(II) dichloride stock solution were added and the absorption at the wavelength maximum of the porphyrin B band was measured.

Langmuir monolayer experiments. π–*A* Isotherms were recorded on a Lauda Filmwaage FW2, which was thermostated at 20 °C and placed in a laminar flow cabinet. Ultrapure water used as the subphase was obtained by filtration through a SERALPUR PRO 90C system. The monolayers were formed by spreading the porphyrins, from their chloroform solutions (10^{-4}–10^{-3} M), on to the water subphase (pH = 5.5) with the help of a microsyringe. After equilibration of the monolayers for at least 15 min the compression was started. The compression and expansion rates were 3 $cm^2\ min^{-1}$. Monolayers were transferred to glass substrates by the vertical dipping technique using a dipping/withdrawal rate of 3 mm min^{-1} before use the substrates were cleaned in a DECON-soap solution by sonication for 15 min. After extensive rinsing with pure water and acetone, the substrates were dried by purging with a stream of N_2. The absorption spectra of monolayers at the air–water interface were recorded with a quartz fibre optic probe (Spectrofip 8452, Photonetics) connected to an HP 8452 diode-array spectrophotometer. The spectrum was taken by passing light through the monolayer and reflecting the light beam back into the fibre, via a concave mirror placed just below the water surface.

Hexaporphyrins in chloroform (10^{-4}–10^{-3} M) were spread on the water surface with a microsyringe. After equilibrating for 5 min, the molecules were compressed with a speed of 10 $Å^2$ per molecule per minute. For the hysteresis experiment the monolayers were compressed until a pressure of 12 mN m^{-1} was reached. This pressure was kept constant for 10 min, after which the barriers were fully expanded. After 30 min, the molecules were compressed again until collapse occurred.

Films of hexaporphyrins were prepared as has been described above. The monolayer was compressed until a pressure of 8 mN m^{-1} was reached, which was kept constant during transfer of the monolayer. Quartz slides of 40×13 mm were cleaned prior to dipping by sonicating in an Alcanox solution for 1 h with subsequent

extensive rinsing with Milli-Q water and sonication in chloroform. The hydrophobic quartz plates were prepared by treatment with a 1% dimethyloctadecyl-3-trimethyloxysilylpropylammonium chloride (DMOAP) solution for 5 min and rinsing with Milli-Q water. Hydrophilic quartz plates were obtained by treatment with a 2:1 mixture of concentrated sulphuric acid and 30% hydrogen peroxide with subsequent rinsing with Milli-Q water. The quartz plates were dipped into the monolayer with a speed of 5 mm min^{-1}.

Electrochemical measurements. Cyclic voltammetry was performed with a PAR Model 173 potentiostat equipped with a PAR Model 176 I/E converter coupled to a PAR Model 175 universal programmer. The measurements were carried out with 1 mM solutions of the porphyrin in dichloromethane with 0.1 M tetrabutylammonium hexafluorophosphate as the supporting electrolyte at 20 °C. A three-electrode configuration was employed with platinum auxiliary and working electrodes and Ag/Ag^+ (0.1 M AgI) as the reference electrode. Potentials were calibrated against the ferrocene/ferrocinium couple ($E_{1/2} = 0.050$ V vs Ag/Ag^+).

Brewster angle microscopy. Brewster angle microscopy experiments were carried out with an NFT BAM1 instrument, manufactured by Nano Film Technology (Göttingen, Germany). The instrument was equipped with a 10 mV He–Ne laser with a beam diameter of 0.68 mm operating at 632.8 nm. Reflections were detected using a CCD camera. Full details of the BAM technique have been described in the literature.[18]

Acknowledgements

The authors thank Roel Fokkens (University of Amsterdam) and Joost van Dongen (University of Eindhoven) for carrying out the field desorption and MALDI-TOF mass spectrometry measurements and Dr P. J. M. van Kan (University of Nijmegen) for carrying out the EPR experiments. This work was supported by the Dutch Foundation for Chemical Research (CW) with financial aid from the Dutch Organisation for Scientific Research (NWO) and the ESF SMARTON programme.

REFERENCES

1. (a) Allen JP, Feher G, Yeates TO, Komiya H, Rees DC. *Proc. Natl. Acad. Sci. USA* 1987; **84**: 5730–5734; (b) Komiya H, Yeates TO, Rees DC, Allen JP, Feher G. *Proc. Natl. Acad. Sci. USA* 1988; **85**: 9012–9016.
2. McDermott G, Prince SM, Freer AA, Hawthornthwaite-Lawless A, Papiz MZ, Cogdel RJ, Isaacs NW. *Nature (London)* 1995; **374**: 517–521.
3. (a) Guengerich FP. *J. Biol. Chem.* 1991; **266**: 10019–10022; (b) Zuber H, Brunisholz RA. In *Chlorophylls*, Scheer H (ed). CRC Press: Boca Raton, FL, 1991; 627–704.
4. (a) Wasielewski MR. *Chem. Rev.*, 1992; **92**: 453–461; (b) Gust D, Moore TA. In *The Porphyrin Handbook*, vol. 8, Kadish KM, Smith KM, Guilard R (eds). Academic Press: New York, 1999; 153–191; (c) Fukuzumi S. In *The Porphyrin Handbook*, vol. 8, Kadish KM, Smith KM, Guilard R (eds). Academic Press: New York, 1999; 115–153.
5. (a) Schenning APHJ, Benneker FBG, Geurts HPM, Liu XY, Nolte RJM. *J. Am. Chem. Soc.* 1996; **118**: 8549–8552; (b) Biemans HAM, Rowan AE, Verhoeven A, Vanoppen P, Latterini L, Foekema J, Schenning APHJ, Meijer EW, de Schyrver FC, Nolte RJM. *J. Am. Chem. Soc.* 1998; **120**: 11054–11060.
6. Jones R, Tredgold RH, Hoorfar A, Hodge P. *Thin Solid Films* 1984; **113**: 115–128.
7. Kroon JM, Sudholter EJR, Schenning APHJ, Nolte RJM. *Langmuir* 1995; **11**: 214–220.
8. (a) van Esch JH, Feiters MC, Peters AM, Nolte RJM. *J. Phys. Chem.* 1994; **98**: 5541–5551; (b) Schenning APHJ, Hubert DHW, Feiters MC, Nolte RJM. *Langmuir* 1996; **12**: 1572–1577.
9. (a) Drain CM, Lehn J-M. *J. Chem. Soc. Chem. Commun.* 1994; 2313–2315; (b) Drain CM, Nifiatis F, Vasenko A, Batteas JD. *Angew. Chem., Int. Ed. Engl.* 1998; **37**: 2344–2347.
10. Smith TD, Pilbrow JK. *Coord. Chem. Rev.* 1974; **13**: 173–278.
11. Palmer G. *Biochem. Soc. Trans.* 1985; **13**: 548–566.
12. Evans IP, Spencer A, Wilkinson G. *J. Chem. Soc., Dalton Trans.* 1973; 204–209.
13. Dandliker PJ, Diederich F, Gross M, Knobler CB, Louati A, Sanford EM. *Angew. Chem. Int. Ed. Engl.* 1994; **33**: 1739–1742.
14. (a) Feiters MC, Rowan AE, Nolte RJM. *Chem. Soc. Rev.*, 2000; 375–384; (b) van Nunen JML. Thesis, Nijmegen, 1995.
15. (a) McRae EG, Kasha M. *J. Chem. Phys.* 1958; **28**: 721–731; (b) Kasha M, Rawls HR, Ashraf El-Bayoumi M. *Pure Appl. Chem.* 1965; **11**: 371–386.
16. Hunter CA, Sanders J. *J. Am. Chem. Soc.*, 1990; **112**: 5525–5535.
17. Coe BJ, Meyer TJ, White PS. *Inorg. Chem.* 1995; **34**: 3600–3609.
18. (a) Hönig D, Overbeck GA, Möbius D. *Adv. Mater.* 1992; **4**: 419–421; (b) Hönig D, Möbius D. *Thin Solid Films*. 1992; **210/211**: 64–68.